COMPARATIVE ANALYSIS OF SIMULATED AND REAL-WORLD INFRARED IMAGES OF SPACE DEBRIS FOR ACTIVE DEBRIS REMOVAL MISSIONS

Naoki Okada[(1)], Shun Okazaki[(1)], Atsushi Okamoto[(1)], Ryo Nakamura[(1)], Toru Yamamoto[(1)]

[(1)] *Japan Aerospace Exploration Agency, 2-1-1 Sengen, Tsukuba, Ibaraki, Japan 305-8505, okada.naoki@jaxa.jp*

ABSTRACT

Infrared (IR) cameras are sensors that observe IR energy emitted from objects. They can provide stable target images regardless of whether in sunlight or eclipse, and are thus a candidate for a navigation sensor for active debris removal (ADR) missions. However, it is difficult to reproduce the in-orbit temperature environment to verify navigation algorithms for an IR camera, so verification is not physically feasible on the ground. Thus, we developed a simulator to simulate IR images obtained in orbit and use them for ground validation.

In 2024, the ADRAS-J satellite developed by Astroscale was used to approach the upper stage of the H-IIA launch vehicle using relative navigation sensors as a part of JAXA's CRD2 Phase-I project. In this study, we compared IR images of the target obtained during its approach with the images from the simulator that had been created prior to the launch of the satellite. Comparing the brightness of the IR images over one orbit, we found that the camera model and the thermal model created before the launch generated simulated images with brightness values close to the actual images.

1 INTRODUCTION

The increase in orbital debris has become a problem, and studies by the Inter-Agency Space Debris Coordination Committee (IADC) and others have suggested the need for ADR [1][2]. In implementing ADR, techniques for approaching the target are required to change the target's orbit. To approach a target, the relative position and orientation of the target from the chaser satellite must be known. LiDAR, a visible light camera, and an IR camera are promising sensors for this purpose. Since each has strengths and weaknesses that depend on the shape of the target, surface characteristics, distance, and environment, these sensors may be combined to realize the mission [3].

Although an IR camera does not directly measure distance like LiDAR, it is a passive sensor that can capture a target from a considerable distance. While visible images depend on the direction of sunlight incident on the target, an IR camera, which mainly captures the temperature of the target, can provide stable navigation data regardless of the presence of sunlight and the direction of incidence since the changes in the image are relatively mild. In Lessons Learned for Orbital Express, IR sensors also increase the robustness of the system against unexpected changes in the light source environment [4]. Thus, an IR camera could be an effective navigation sensor for ADR missions.

Nevertheless, it is not easy to validate the navigation algorithm for the IR camera by pre-launch ground tests [5] because it is difficult to image the temperature distribution of the target and the background space temperature with an IR camera according to in-orbit conditions. Therefore, we propose using simulated images for ground tests of IR camera navigation [6][7].

Many previous efforts to simulate IR camera images assumed ground scenes taken from above [8][9]. The creation of simulated IR images of orbiting artificial objects has also been studied [10]. No study has shown how well the simulated images created in these studies reproduce actual images obtained in orbit.

This study used the actual IR images of orbital debris obtained by CRD2 Phase-I. This paper presents our analysis of the quality of the images generated by the proposed IR image simulator.

Section 2 presents an overview of this simulator. Section 3 summarizes the analysis of the IR images taken by CRD2 Phase-I from the viewpoint of the camera model. Section 4 compares and analyzes simulated and actual images from the viewpoint of the thermal model. Finally, Section 5 presents our conclusions.

2 SIMULATOR

Fig. 1 gives an overview of the simulator. The simulator takes the geometry model, thermo-optical properties, and surface temperature of the object as input, and generates a simulated IR image of arbitrary relative position and orientation. The surface temperature was derived from a thermal analysis by Thermal Desktop® [11], a tool commonly used in spacecraft design. The simulated IR energy incident on the camera elements was calculated from the IR emission and reflection models, and the output IR image was obtained by calculating the intensity for each pixel's gain, offset, and noise characteristics.

Proc. 9th European Conference on Space Debris, Bonn, Germany, 1–4 April 2025, published by the ESA Space Debris Office

Editors: S. Lemmens, T. Flohrer & F. Schmitz, (http://conference.sdo.esoc.esa.int, April 2025)

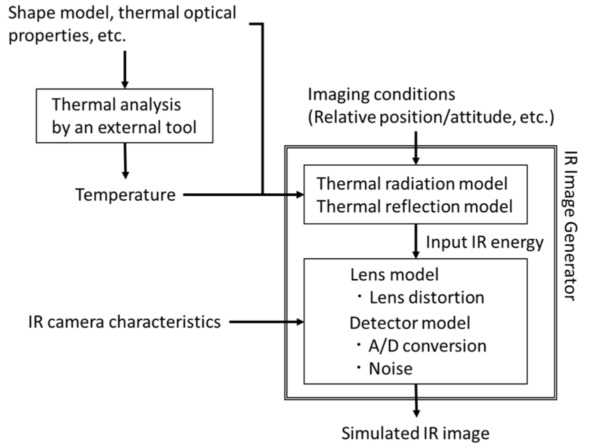

Figure 1. Simulator overview

A thermal model of the target is also required to create a simulated IR image. A per-pixel gain, offset, and noise model was created for the camera model from image data of a temperature-controlled blackbody captured by an IR camera. A modified version of the thermal model created from the design information was used, considering the varied thermo-optical properties of orbiting debris.

3 OVERVIEW OF OBSERVED IMAGES

The CRD2 Phase-I target is an upper stage of the H-IIA rocket that launched GOSAT in 2009. This cylindrical target, 11 m long and 4 m in diameter, is in a circular orbit at an altitude of around 600 km and an inclination of 98 degrees. The target consists of several parts from the Payload Attachment Fitting (PAF) to the nozzle, as shown in Fig. 2. Most of the parts are metal surfaces, except the Poly Isocyanate Foam (PIF) insulation, which is a non-metallic surface.

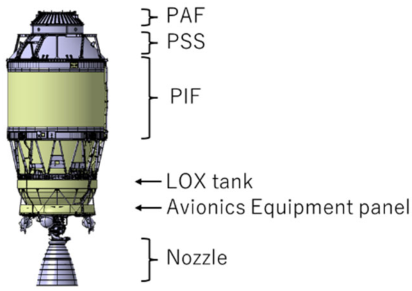

Figure 2. Target: rocket's upper stage

The ADRAS-J satellite in CRD2 Phase-I performed relative navigation based on multiple sensor measurements from several kilometers to this target and conducted close-proximity operations to the target. The visible light images of the fixed-point observation at 50 m and the fly-around observation are available. These show the target maintains a gravity-gradient-stabilized attitude with the PAF side toward the center of the Earth, with almost no rotation around the long axis of the body.

IR images were taken during the relative navigation approach, as shown in Fig. 3, for representative images taken in sunlight and in eclipse.

Figure 3. IR camera images during sunlight (left) and eclipse (right)

The PIF has a high emissivity and is easily seen in the IR image; the temperature change between sunlight and eclipse sides is clearly seen. Other areas are largely bare metal surfaces or covered with MLI. These have low emissivity and are difficult to see in the IR image, but the PAF side, which always faces the Earth, receives heat input from the Earth and appears relatively bright in the eclipse. The Payload Support Structure (PSS) and the nozzle show the Earth in the image as a mirror image.

4 EVALUATION OF CAMERA MODEL

This section discusses the features of the IR camera obtained from the in-orbit images.

4.1 Background

The captured images showed a change in overall brightness over time. This change included both continuous changes and discrete jumps. These were attributed to changes in intensity due to variations in the camera's temperature and the brightness compensation function inside the camera. To evaluate the changes in the intensity value of the target, it is necessary to remove this variation in the background value.

4.2 PSF estimation

Image sharpness is important in relative navigation using IR imaging. The images taken by ADRAS-J, show a phenomenon in which target's brightness shows an apparent extension into the deep-space background. Thus, the Point Spread Function (PSF) in this image was estimated from the brightness change of the PIF and deep-space edges, which have the brightest and straightest edges in the image (Fig. 4). Using multiple rows of edge data from an image with tilted edges, the intensity value change was read before and after the edge in sub-pixel units. Spline interpolation was performed, and the Line Spread Function (LSF) was obtained using first-order differentiation.

The PSF was assumed to be independent and the same for each axis. Since the intensity on the PIF side was not constant, there was a significant variation in each row, and the LSF was created using data from only the deep-space side of the edges and folded back.

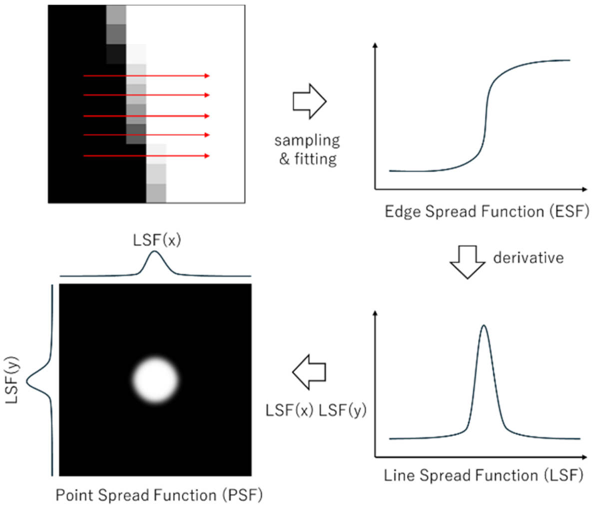

Figure 4. PSF estimation

Using the PSF obtained this way, an image without blurring due to PSF can be estimated using Wiener deconvolution. Fig. 5 shows the original and processed images side by side. Although details have some artificial noise, the overall image is sharp.

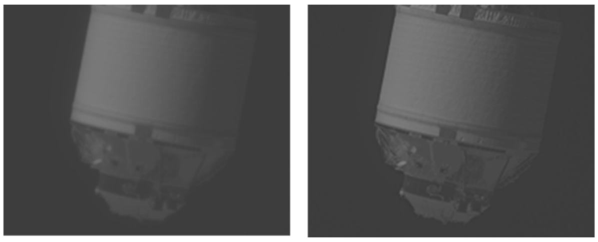

Figure 5. Wiener deconvolution (left: original, right: processed)

4.3 Intensity calibration

Even if the sensitivity of the IR camera is examined by photographing a temperature-controlled blackbody before launch to determine the relationship between blackbody radiance and temperature, the sensitivity may change due to environmental changes after launch or over time. Here, we consider calibrating the camera by photographing an object with a known brightness temperature in orbit. We consider the Moon an object whose brightness temperature is relatively stable and known. Ref. [12] shows a plot of the brightness temperature of the Moon by latitude and LST with standard deviation. The range of latitude 0–60 degrees and LST 9–15, where the standard deviation is suppressed to about 10K, was spline-interpolated (Fig. 6), and the relation with the intensity values for the Moon taken by the ADRAS-J camera (Fig. 7) was obtained (Fig. 8). By comparing this result with the sensor model created in advance, it is possible to evaluate changes in sensor characteristics.

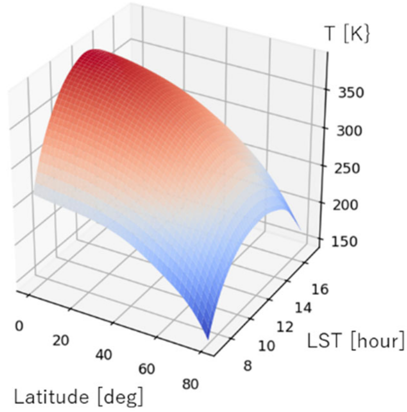

Figure 6. Lunar surface brightness temperature obtained by interpolation from [12]

Figure 7. IR image of the Moon

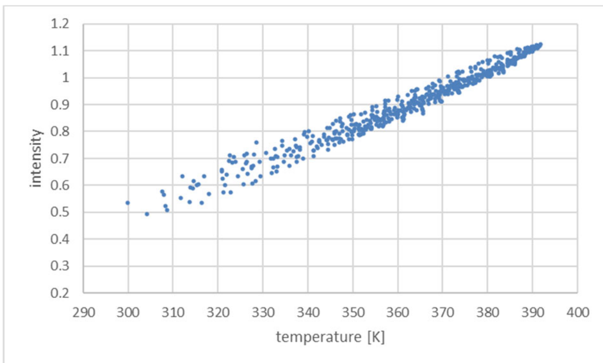

Figure 8. Relationship between brightness temperature and intensity value

5 EVALUATION OF THERMAL MODEL

This section evaluates how adequately the thermal model created before launch simulated the actual temperatures of an orbiting target. The IR images used for comparison were taken at 24-second intervals between 10:20:01 and 12:06:01 on June 17, 2024. In the image sequence at this period, the target was photographed from behind the orbit, with the Earth at the bottom of the image for one orbit. It started with the sun beginning to hit the target from the back side of the target, then the sun moved behind the camera, went into the eclipse, and then into the sunlight again. Thermal analysis was based on Thermal Desktop® with the same target orbits and thermal input conditions at that time, and the results were used to generate an image using the IR image simulator. Fig. 9 shows actual and simulated images at the same time. Next, we extracted and compared the time variation of the intensities of each part of the target from the actual and simulated image sequences. Since the time variation of the intensity in the actual image included the offset shown in Section 4.1, we corrected it so that the intensity of the background was constant. The simulated image does not reflect this time variation, but the intensity of the background was corrected to match that of the actual image with a constant value that did not depend on time. However, the calibration described in Section 4.3 is not applied here.

Fig. 10 shows the profile of intensity between the actual and simulated images for the PAF, PSS, PIF, MLI, and the nozzle. The minimum and maximum intensities for the PAF are almost the same. The increased intensity in sunlight is also reasonably consistent, but the simulated image shows the decreased intensity accelerating. Two areas on the PSS in the actual image were compared: one where the Earth was reflected, the other where it was not (i.e., in the shadow of the small satellite base). The point with the reflection of the Earth shows a significant change in brightness because it reflects the pattern of the Earth below, from time to time. However, the simulated image did not show the fine intensity variations seen in the actual image because the Earth's reflection was simulated as a constant value. The actual image also showed little intensity variation throughout the orbit where the Earth was not reflected, so the simulated intensity showed a reasonable variation when the Earth's reflection was considered a constant. The overall PIF variation in both types of image was generally consistent. However, the rise and fall in intensity in the simulated image was slower than in the actual one, and the maximum intensity is also smaller. This may be due to the smaller heat capacity and higher solar absorptivity of the actual object compared to the thermal model. For the area covered by the MLI, the actual image shows more intense changes and higher intensity overall. This difference is thought to be caused by the fact that the MLI areas also have a strong reflection of the Earth, and the actual image also shows a pattern that seems to originate from the unevenness of the MLI. For the nozzle, the actual image shows a more significant change in intensity than the simulated image, and this is the area where the difference between the simulated image and the actual image is greater. One factor may be that the thermal model represents the nozzle as a simple plate, so the heat capacity is higher due to the difference in thickness and other factors.

Another difference between the overall appearance of the actual image and the simulated image is that the wrinkles of the MLI, fine parts, and textures are clearly visible in the actual image. These details are not visible in the simulated image because they are not built into the thermal model.

The primary purpose of creating the target thermal model and the IR image simulator in this study was to perform pre-launch ground verification of the relative position and attitude estimation algorithm using an IR camera. The fact that the brightness variation on the image for each part of the target could be assumed to some extent before launch indicates that verifying the navigation

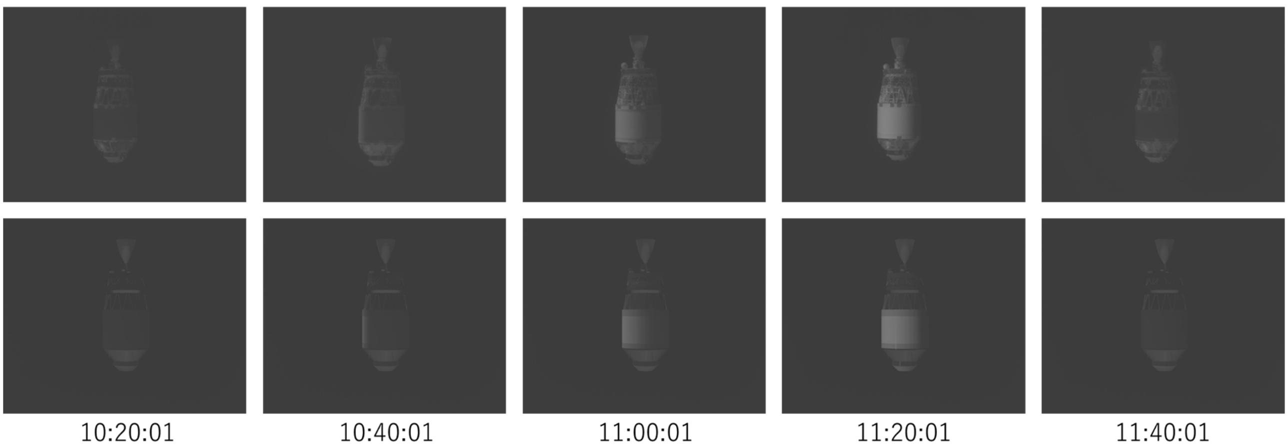

Figure 9. Time-series variation of actual (upper row) and simulated (lower row) images

algorithm on the ground with simulated images is advantageous. On the other hand, the lack of prior reflection of image blurring, which also affects image processing, is an area for improvement.

In addition, the thermal design of the chaser satellite must also consider the thermal model of the target in order to grasp and change the orbit of the target in the ADR mission. It may not be able to simulate the temperature state of a target that has been in orbit for several years with the thermal model at the time of design. The validity of the thermal model prepared in advance in this study provides important insights into how to create a thermal model of in-orbit debris.

When the thermal model of the upper stage of the rocket was prepared prior to launch, the same values as those used in the design were used for the thermo-optical properties of the metal parts, while the thermo-optical properties of the insulation material were set to reflect the results of accelerated ultraviolet (UV) exposure tests of the material, because it was considered that the material would degrade significantly due to UV radiation.

The image brightness obtained in an IR image represents the incident IR energy for each pixel and is the product of the IR emissivity and blackbody temperature of the target surface projected on the pixel, excluding the reflected component. In other words, the object's temperature cannot be determined if the emissivity is

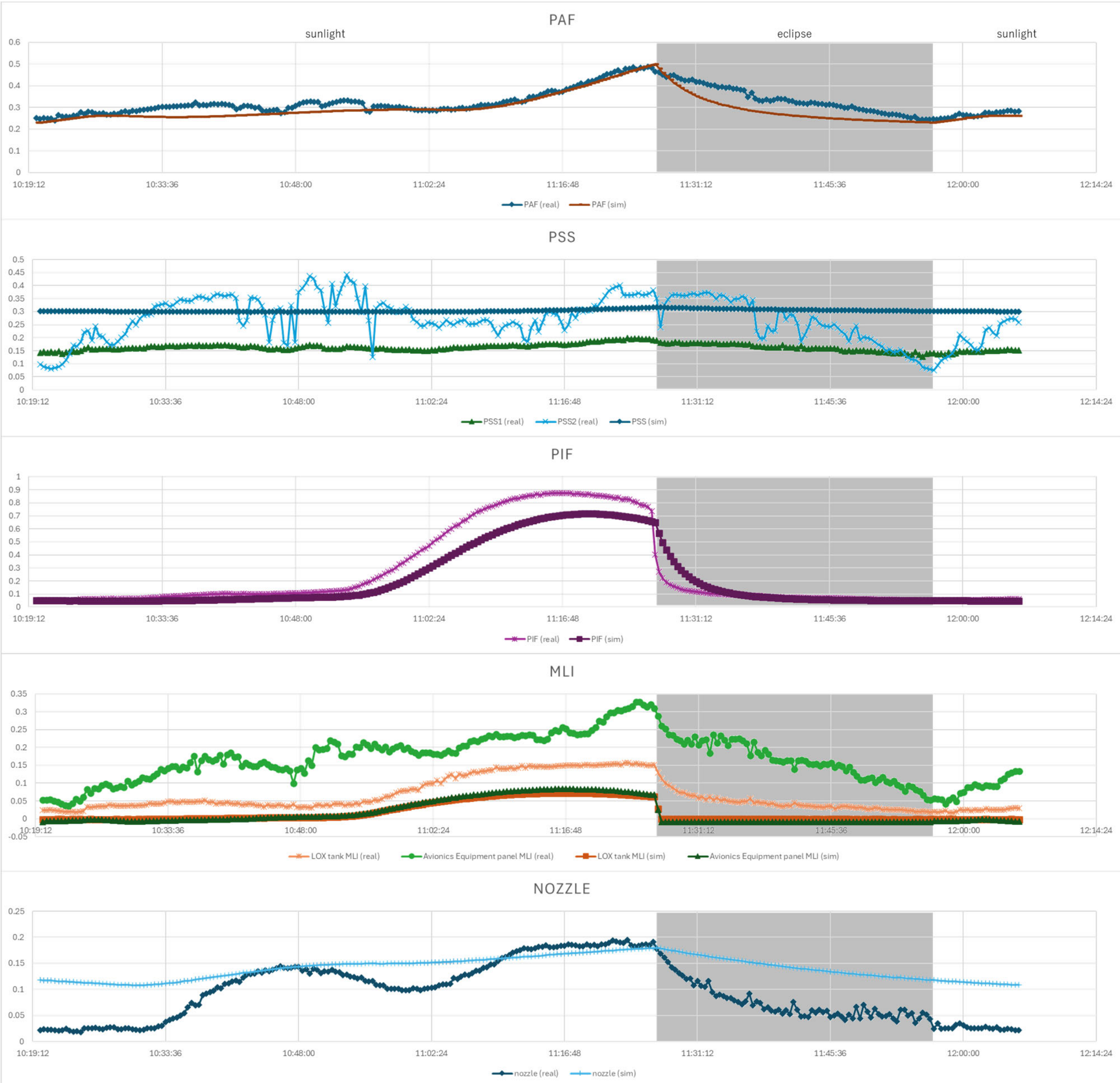

Figure 10. Comparison of actual and simulated images of time-series intensity profiles at each part of the target

unknown. Thus, it is not possible to fully correlate the thermal model from the captured IR images alone. However, the image brightness profile of each area obtained in this study is consistent overall, so the thermal model is closely aligned with reality. In other words, the thermal modeling policy for a target, which has been in orbit for more than ten years was generally appropriate: the thermo-optical properties of the metal parts have not changed significantly since before launch, and those of the insulation material have deteriorated to UV rays.

6 CONCLUSION

We propose a method using simulated images to minimize the difficulty of reproducing the temperature environment in ground validation, an issue when using an IR camera as a relative navigation sensor in ADR missions. This paper shows that the simulator can effectively verify a navigation algorithm by comparing actual images obtained in orbit with simulated images. Since the simulation could not represent some differences from actual images, devising a simulator with an appropriate level of detail and fidelity according to the navigation algorithm is important. In the future, we plan to develop simulators that simulate the image features seen in the actual images more completely and accurately.

7 ACKNOWLEDGMENTS

We would like to express our appreciation to Astroscale Japan, which developed and operated the ADRAS-J satellite as a contract partner of the JAXA CRD2 Phase-I project and provided in-orbit IR images.

8 REFERENCES

1. Liou, J.-C., Anikumar, A.K., Bastida Virgili, B., Hanada, T., Krag, H., Lewis, H., Raj, M.X.J., Rao, M.M., Rossi, A. & Sharma, R.K. (2013). Stability of the future LEO environment – an IADC comparison study, *Proc. 6th European Conference on Space Debris*.

2. Liou, J.-C., Johnson, N.L. & Hill, N.M. (2010). Controlling the growth of future LEO debris populations with active debris removal, *Acta Astronautica*, Volume 66, Issues 5–6, pp. 648–653.

3. Yamamoto, T., Murakami, N., Nakajima, Y. & Yamanaka, K. (2014). Navigation and Trajectory Design for Japanese Active Debris Removal Mission, *ISSFD 2014*.

4. Dennehy, C.J. & Carpenter, J.R. (2011). A Summary of the Rendezvous, Proximity Operations, Docking, and Undocking (RPODU) Lessons Learned from the Defense Advanced Research Project Agency (DARPA) Orbital Express (OE) Demonstration System Mission, NASA/TM-2011-217088, NESC-RP-10-00628.

5. Schnizer, F., Sonnenburg, A., Janschek, K. & Gestido, M.S. (2017). Lessons-learned from On-ground Testing of Image-based Non-cooperative Rendezvous Navigation with Visible-spectrum and Thermal Infrared Cameras, *ESA GNC 2017*.

6. Okada, N., Hidaka, M., Negishi, H., Nakajima, Y., Sasaki, T. & Yamamoto, T. (2022). Infrared image generator of artificial space object for verifying relative navigation in rendezvous, *IEEE Aerospace Conference 2022*.

7. Okada, N. & Yamamoto, T. (2023). Simulating Realistic Infrared Images with Noise for Navigation Algorithm Verification in Active Debris Removal Missions, *2nd International Orbital Debris Conference*.

8. Guissin, R., Lavi, E., Palatnik, A., Gronau, Y., Repasi, E., Wittenstein, W., Gal, R. & Ben-Ezra, M. (2005). IRISIM: Infrared Imaging Simulator, *Proceedings of the SPIE*, Volume 5784, pp. 190–200.

9. Poglio, T., Savaria, E. & Wald, L. (2002). OSIRIS: A Simulator of Outdoor Scenes in Thermal Infrared Range, *ISPRS Commission III Symposium "Photogrammetric Computer Vision,"* pp. 240–245.

10. Martin, I., Dunstan, M., Vural, D. & Gestido, M. S. (2021). Simulating thermal infrared images of planets, asteroids and spacecraft, *ESA ICATT 2021*.

11. C&R Technologies, Inc. Thermal Desktop®: https://www.crtech.com/products/thermal-desktop

12. Williams, J.-P., Paige, D.A., Greenhagen, B.T. & Sefton-Nash, E. (2017). The global surface temperatures of the Moon as measured by the Diviner Lunar Radiometer Experiment, *Icarus* 283, pp300-325.